CHEMISTRY OF MATERIALS

pubs.acs.org/cm

Methods/Protocols

The Autonomous Formulation Laboratory: An Open Liquid Handling Platform for Formulation Discovery Using X-ray and Neutron Scattering

Peter A. Beaucage* and Tyler B. Martin*

Cite This: *Chem. Mater.* 2023, 35, 846–852

Read Online

ACCESS | Metrics & More | Article Recommendations | Supporting Information

ABSTRACT: The application of machine learning techniques to X-ray scattering experiments has been of significant recent interest, offering advances in areas such as the study of complex oxides. Despite these success stories, few applications of these techniques into soft materials have been reported, likely due in part to the highly nonequilibrium nature of soft materials phase spaces and the complexities associated with autonomous formulation preparation. Here, we report the design of the Autonomous Formulation Laboratory, a robust platform for the automated synthesis and measurement of complex liquid mixtures using X-ray and neutron scattering, readily extensible to system-specific complementary techniques such as spectroscopy and rheometry. We describe the application of the platform to generate dense, highly reproducible data sets on material systems ranging from silica nanoparticles to block copolymer micelles. We expect the platform to prove revolutionary to the understanding of the stability of complex liquid formulations and the resulting data sets to provide fertile ground for the development of machine learning techniques for complex soft materials phase spaces.

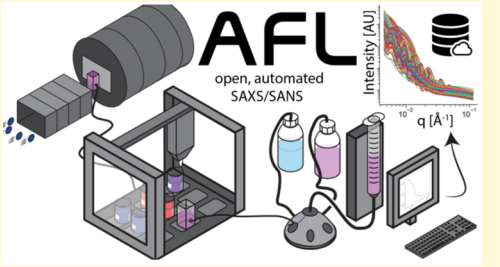

INTRODUCTION

Complex liquid mixtures are the foundation of industries ranging from personal care products to biotherapeutics to specialty chemicals. In many such applications, maintaining a specific, targeted phase is crucial to application performance, and small variations in formulation composition can result in phase changes that destroy desirable aspects of performance. Whereas phase targeting generally occurs in product development, changes in formulation composition are frequently made as products are engineered for manufacturing, with sometimes unexpected impacts on product performance. Neutron and X-ray scattering (SANS and SAXS) are workhorse techniques for characterizing *model* formulations, but the large number of components in many real products makes exhaustive mapping of the parameter space impossible because of the sheer number of possible compositions. To enable rational design of these materials, we must leverage machine learning (ML) tools to greatly reduce the expense of creating structure−composition maps (phase diagrams). Leveraging machine learning (ML) tools, researchers can instead intelligently explore parameter space to greatly reduce the cost of creating structure−composition maps (phase diagrams), enabling the rational design of these materials.

Machine learning techniques such as neural networks, Bayesian optimization, and other strategies have revolutionized fields from natural language processing to machine vision and have been applied to great effect in the analysis of scientific data for imaging techniques.[1−3] The application of such techniques to reciprocal space (scattering) data processing is, by comparison, in its infancy.[4−8] The main obstacle to the translation of machine learning techniques from imaging data to scattering data is the lack of sufficient quantities of well-tagged measurements for training and algorithm development. Deep learning techniques such as convolutional neural nets have shown substantial promise for classification of SAXS and SANS images, but the data used to train the net is typically largely simulated because as many as 10^6 images or more are required. When typical synchrotron exposure times are used, this quantity of data could be collected in just over 2 days (a typical single-user allocation), but generation of 100,000 unique samples with well-described and systematic variation in composition would represent a Herculean effort. Although some success has been achieved in generating high-density data sets, in particular with both spatially resolved processing and combinatorial composition variations in inorganic materials, these techniques are inherently tied to thin films and thus prevent the exploration of bulk liquid mixtures.[9,10]

Both the development and application of ML tools requires a platform capable of autonomously creating samples with varying composition and chemistry. Although there are numerous examples of robots that perform specific user facility operations,

Received: October 12, 2022
Revised: January 5, 2023
Published: January 24, 2023

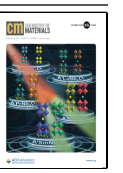

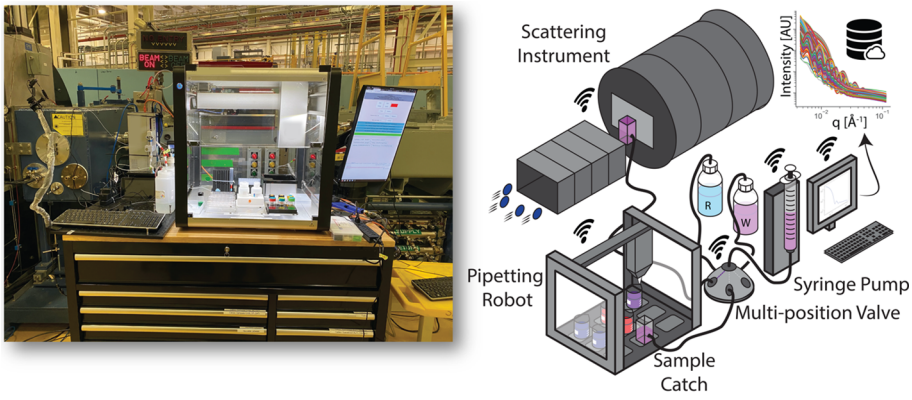

Figure 1. Photograph and schematic of AFL.

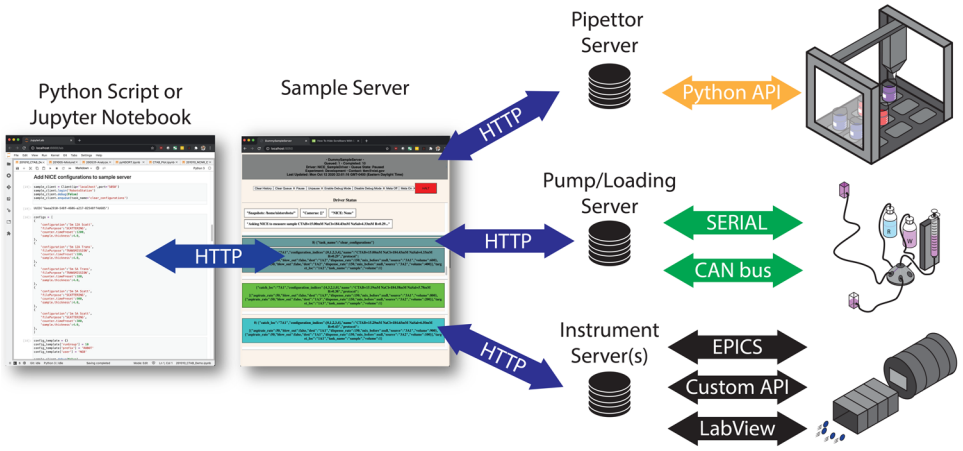

Figure 2. Schematic of server architecture of AFL.

these systems tend to be bespoke and nonadaptable to new tasks.[11−13] We have developed a highly adaptable, open sample platform that can be programmed to autonomously prepare and characterize liquid formulations, which in addition to ML-assisted search, will be used for mail-in operations and reference data set generation.

The goal of our system, called the Autonomous Formulation Laboratory (AFL), is to prepare samples from stock solutions and characterize their structure using any number of techniques, centering around neutron and X-ray scattering but also including complementary techniques such as optical imaging, ultraviolet−visible−near-infrared (UV−vis−NIR) spectroscopy, viscometry, and densiometry. The base platform consists of commercial off-the-shelf components (see disclaimer) including an automated pipetting system, syringe pumps, flow selectors, and flow cells/capillaries (Figure 1). The components are orchestrated by a straightforward but highly adaptable Python microservice software platform that greatly simplifies integrating new in-line devices (e.g., flow mixers), secondary measurements (e.g., UV−vis−IR spectroscopy), or other sample environments (e.g., Capillary RheoSANS).[14] We expect this open platform for multimodal, highly automated sample preparation will enable new operational paradigms for user facility-based techniques.

PHYSICAL SYSTEM DESIGN

The overall design concept of the system (Figure 1) is straightforward: a commercial autopipetting robot (Opentrons OT-2), with available pipet volumes ranging from 1 μL to 1 mL, is used for solution preparation. The robot prepares a specified sample from stock solutions, mixes the sample using pipet mixing in a mixing well, and then transfers an aliquot of the sample to a custom sample catch outfitted with integrated stirring. The catch is connected via $^{1}/_{16}$ in. thin-wall ethylene tetrafluoroethylene (ETFE) tubing and $^{1}/_{4}$ in.-28 flangeless fittings to a loading system that consists of a 10-to-1 multiposition valve (Vici Components C25-3180EUHB) and a syringe pump (Cetoni neMeSys 110). When commanded to load, the system changes the valve position to the catch, withdraws an appropriate amount to bring the sample into the syringe barrel, then changes the valve position to the measurement cell, and dispenses an appropriate volume to place the sample at the measurement position. The specific measurement cell design depends on the measurement, ranging from thin-walled capillaries for SAXS to custom quartz cuvettes for SANS and UV−vis−NIR. In-line measurements (UV−vis−NIR, etc.) are triggered automatically at the beginning of the dispensing action and measured continuously as the sample flows past. At the end of the measurement, the sample is pushed through the sample cell and into a waste bottle. Alternately, the sample can be drawn back into the syringe and sent back to the catch for further analysis, though it should be noted that in the case of SANS measurements this mode is not used because of potential neutron activation of the sample.

Maintaining the system free of intersample interference is of the utmost importance in autonomous measurements. To that end, the system is connected to 1 L bottles of a rinse solvent

https://doi.org/10.1021/acs.chemmater.2c03118
Chem. Mater. 2023, 35, 846−852

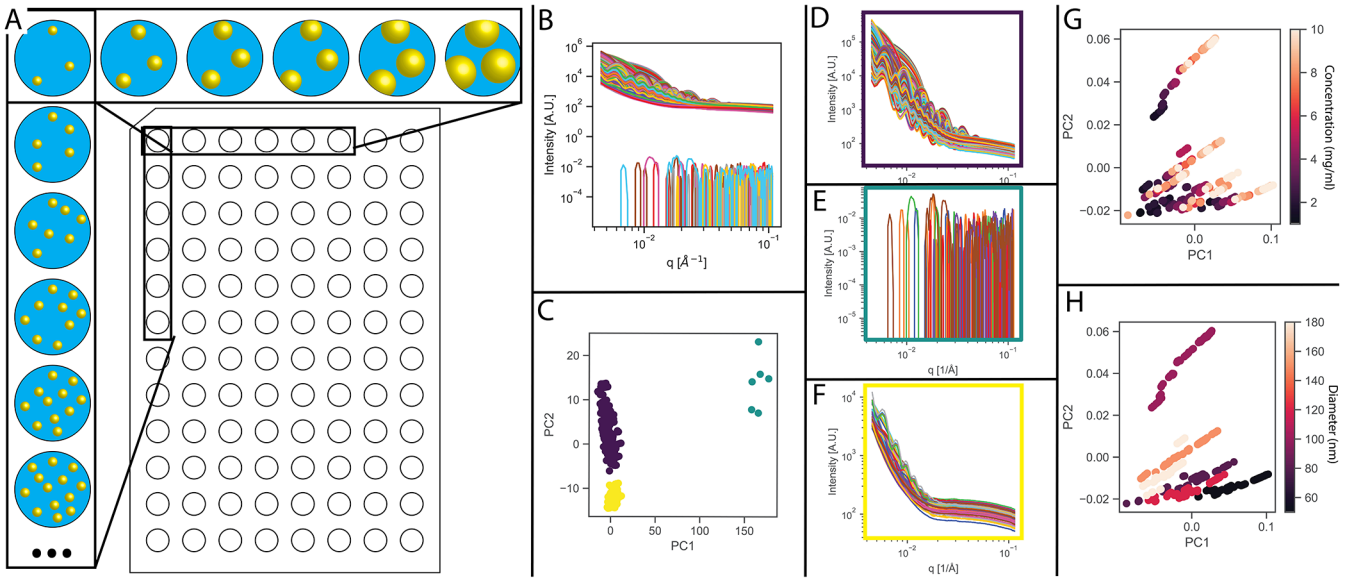

Figure 3. (A) Schematic showing the solution composition axes explored in the experiment, nanoparticle concentration (vertical in schematic), and nanoparticle diameter (horizontal in schematic). Note that in the actual experiment the samples were prepared sequentially and in random order to minimize the contribution of systematic error; the geometric layout is simply a conceptual illustration. (B) SAXS data and (C−H) PCA analysis of SiO_2 nanoparticle solutions. Part C shows the projection of the scattering data onto the first two principal components and parts D−F show the scattering patterns associated with each of the clusters in part C. Parts G and H display the PCA projection of the data in part D, colored by particle concentration (G) and particle diameter (H).

(chosen depending on the system to be studied, but typically a 1:1 volume ratio of water and ethanol). After a sample is loaded, the system automatically withdraws a plug of rinse solvent from the tank and flushes the tubes leading to the catch with it, before automatically discharging to a separate waste bottle. Similarly, after a measurement, the system automatically pushes several pulses of rinse solvent through the measurement system. The system is also connected, via a separate valve, to a low-pressure supply of filtered nitrogen gas. After the sample position is rinsed, the cell is briefly connected to nitrogen to push out any remaining bulk liquid plugs and dry any residual solvent on the cell and tubing walls.

Further details on the system design are given in the Supporting Information and open hardware designs are available on GitHub at https://www.github.com/usnistgov/AFL-hardware.

SOFTWARE ARCHITECTURE

The physical design of the robot is supported by a highly extensible Python microservice backend. Each device or group of devices (e.g., syringe pump + flow selectors) is encapsulated in a Python-based server that provides a command language, as shown by the schematic in Figure 2. The progress of an experiment can be monitored by the interactive web pages generated by each server, or by a separate web application that gathers the output from all the servers into a single interface. The granularity of the command language for each device server is arbitrary and is defined using simple Python classes. Users can define commands that map directly onto device operations (e.g., move flow selector to port 8) or complex composite commands involving multiple devices (e.g., perform a multicycle rinse routine). All commands to device servers are transmitted as HTTP web requests, allowing our system to operate on existing networks. By separating device groups into different device servers, we allow for asynchronous operations so that rinsing, sample preparation, and sample measurement can occur simultaneously. Another substantial advantage is that equipment with wildly differing interfaces can be connected on a common platform. For example, our current syringe pump interfaces via a custom CAN-based communications protocol, whereas the interface to our laboratory-scale SAXS instruments is via LabVIEW. Such interfaces are abstracted and encapsulated behind device servers, such that the sample preparation engine (and ultimately the user) have no need to know the low-level details.

Users design experiments on the platform by writing Python scripts or Jupyter notebooks. The user interface is through simple, physical commands, such as “load” and “measure”, and the user does not interact with communication or operational details. After the system is initialized, users simply request a specific sample composition be measured, and the sample server orchestrates all details associated with sample preparation, transfer, measurement, and cleanup. For more specific control, users can also interface with all device servers directly. For SANS experiments at the NCNR, the neutron instrument is entirely controlled in the script via a custom scripting interface, whereas our laboratory SAXS is interfaced through a Python interface to LabVIEW. A common command set is used in the open-source software package and adhered to for device server drivers; for example, all supported syringe pumps share common software commands regardless of the underlying protocol, and all scattering instruments—whether synchrotron-based, laboratory-based, or neutron—can be addressed in the same way. This adherence to common protocols minimizes the effort needed to connect the system to different facilities and builds toward a “write once, run anywhere” paradigm for user experiment workflows.

To enable autonomous formulation exploration driven by ML, we further developed a Python library that abstracts the sample preparation process (available open-source at https://

https://doi.org/10.1021/acs.chemmater.2c03118
Chem. Mater. 2023, 35, 846−852

github.com/usnistgov/afl-automation). Users specify the location and composition of stock solutions along with the composition of desired samples. The library then solves the mass balance equations and creates a pipetting protocol, taking into account the uncertainty of the transfers and allowing for nonexact but best achievable matches to target compositions. Users can specify desired samples by the component mass, volume, or scattering length density, enabling the trivial construction of concentration or contrast-variation series. Most importantly, this sample abstraction will enable future ML algorithms to specify points in composition space without needing user intervention during the autonomous phase-space mapping.

All measurement data in our system is stored and tagged with a rigorous adherence to FAIR data principles.[15] The sample preparation engine described above is coupled into a database designed to track the provenance of measured samples all the way back to the raw materials that were used to create stock solutions. This process is supported by a web application that allows users to generate scannable labels that can be affixed to raw materials or prepared solutions. The web application can read the measured mass from a connected balance, enabling a paperless and precise workflow for creating stock solutions. During an autonomous run, the sample preparation server will populate the database with sample metadata and link this metadata to the metadata of the stock solutions used to create the sample. Further software details and documentation are given in the Supporting Information and the full AFL-automation package is available on Github (https://www.github.com/usnistgov/AFL-automation).

DEMONSTRATIONS

As a first demonstration of the system, we performed a dense series of X-ray scattering measurements of SiO_2 nanoparticle standards (Figure 3). The system was preloaded with 10 mg/mL solutions of a series of low-dispersity particles with diameters ranging from 50 to 180 nm (Figure 3A). The system was programmed to dilute each particle into water for final concentrations ranging from 1 to 10 mg/mL, supplied with appropriate consumables, and allowed to run for about 8 h unattended.

The resulting SAXS patterns are shown in Figure 3B. The density of this data set, coupled with the common preparation platform, is expected to be a fertile ground for training of machine-learning-based approaches to scattering data. As a first proof of principle for such data sets, we used principal component analysis (PCA) coupled with agglomerative clustering to perform unsupervised classification of the data (Figure 3C). The first classification pass identified several conditions that were obvious measurement errors—a bubble was introduced into the measurement capillary (Figure 3F), the synchrotron was performing beam orbit corrections (Figure 3E), and so forth. Isolation of the "good data" cluster (Figure 3D) and a second application of PCA resulted in the separation of the samples into components that correlate with the known, ground-truth concentration (Figure 3G) and diameter (Figure 3H) data. The correspondence between physical parameters and observed component values suggests that, given rich training data, unsupervised techniques might be of significant utility for rapid, online analysis of scattering data. Additionally, the first PCA pass, especially combined with feature engineering to include, for example, the storage ring orbit parameters, incident beam flux, and measured sample transmission, could provide valuable real-time feedback to a measurement to allow it to autonomously identify and correct erroneous measurements without user involvement.

Moving beyond simple dilution experiments, we used SANS measurements in the AFL to study the impact of salt and sodium salicylate addition upon the micellization of cetyltrimethylammonium bromide (CTAB, Figure 4), both to demonstrate the versatility of the AFL platform for both X-ray and neutron scattering measurements and to highlight the data density and reproducibility that can be obtained using the AFL—moving beyond snapshots to understand the continuum of the phase space. The CTAB−salicylate−salt system and its analogues are one of the most studied micellar systems in the soft-matter rheology community because of the rich relationship between the microstructure evolution of the system and its linear/nonlinear viscoelastic behavior.[16,17] To run this experiment in the AFL, six aqueous stock solutions (CTAB, CTAB + NaCl, CTAB + salicylate + NaCl, salicylate, NaCl, and pure water) were loaded into the AFL, and the system was programmed with the exact concentrations of the stock solutions. The AFL's mass balance solver automatically converts chemical space concentrations and higher-order composition coordinates, such as the ratio R of salicylate to CTAB, into transfer volumes of each given stock solution. These transfers are then executed by the pipettor,

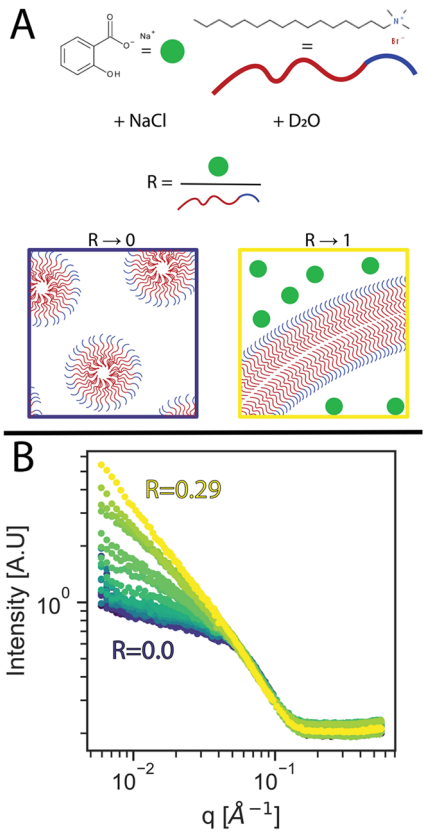

Figure 4. (A) Schematic showing the chemistry of the CTAB (chain), sodium salicylate (green dot), NaCl, and D_2O system studied, where the ratio R is the concentration of salicylate relative to that of CTAB. At low values of R the system forms spherical micelles, which transition to extended wormlike micelles at higher R-values. (B) SANS data of the system under study, colored by the value of R. A shift of the low-q slope of the data from near flat to a q^{-1} scaling is consistent with elongation of the micelles in a spherical-to-wormlike transition.

https://doi.org/10.1021/acs.chemmater.2c03118
Chem. Mater. 2023, 35, 846−852

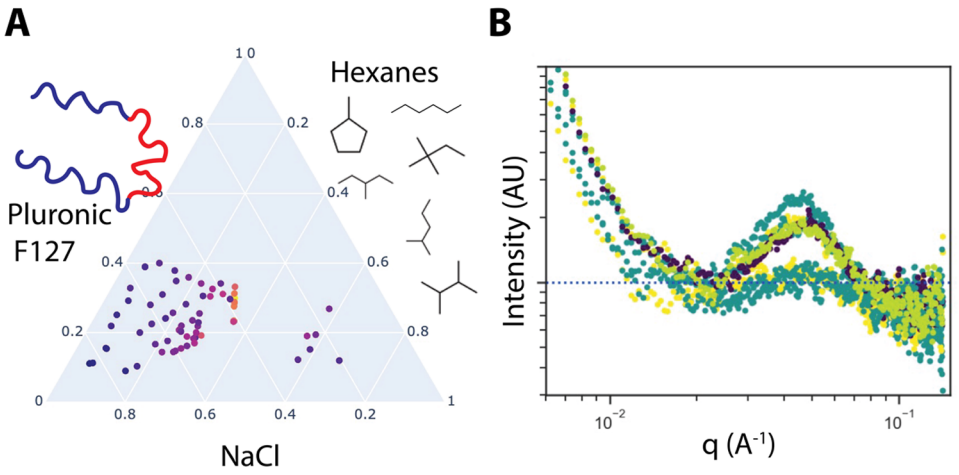

Figure 5. (A) Ternary phase diagram and (B) selected SAXS data for a system composed on Pluronic F127, NaCl, hexanes, and water. Each data point on the phase diagram in (A) represents an individual SAXS measurement in (B), where the color of the point in (A) indicates the intensity of the diffraction peak at $q = 0.045$ A^{-1}, consistent with the development of micelle−micelle packing in the F127 solution. The colors in (B) are simply to distinguish the datasets from one another.

pipet mixed, and the resulting solution pumped into a neutron measurement cuvette—all without human intervention. With increasing concentration, the bulky salicylate counterion interacts with the micelle and causes a transition from spherical to wormlike micelle structures, as shown schematically in Figure 4A. In Figure 4B, we not only confirm that we observe the transition in automatically prepared samples but also see that this transition is continuous, with the data smoothly varying from a spherical form factor at low salicylate concentrations to displaying the classic rodlike power law ($I \sim q^{-1}$) at higher concentrations. These data can be modeled to calculate the shape distribution of the micelles as it shifts from purely spherical to purely rodlike. If coupled to an inline rheometer, the AFL could simultaneously collect viscometric and SANS data to better understand the quiescent structure−viscosity relationship in this system. Taking this a step further, the open hardware and software architecture of the AFL enables it to be readily coupled to cutting edge instrumentation, such as the Capillary RheoSANS,[14] allowing it to *simultaneously* measure the structure and the full rheological response. As demonstrated in the nanoparticle example above, this density of data coupled with unified, highly stable sample preparation and measurement protocols will enable the application of machine-learning techniques that have the potential to unlock new physics and new understanding.

Finally, a primary motivation for developing the AFL was to aid in the study of industrial liquid formulations. Poloxamer-based formulations form the foundation for many products from applications in drug delivery to cosmetics to consumer products. In Figure 5B, we show laboratory SAXS data acquired using the AFL platform for a system containing F127, hexanes, salt, and water. This system is a reasonable model for many surfactant−oil formulations encountered across industry and academia, from fragrance loading in personal care products to preservatives in drug delivery. To measure the system in the AFL, we prepared stock solutions of each component in a similar manner to the surfactants in Figure 4 (*vide supra*). The partial coverage of the phase diagram with experimental points is reflective of the bounds imposed by the concentrations of these stock solutions and physical limitations of the measurement (e.g., maximum and minimum pipet transfer volumes and viscosity). The AFL software automatically calculates these bounds and confines studies appropriately. After stocks are loaded, the AFL independently solves a mass balance for a user-requested composition, calculates the transfers needed from each stock solution, pumps the sample into the X-ray measurement cell, and triggers a SAXS exposure with a typical exposure time of 1 h on our in-house instrument. With varying composition, we see that a diffraction peak appears, indicating that the system has formed highly ordered micelles. Figure 5A shows the locations of this peak in composition space in the form of a ternary phase diagram with the color of each point set by the height of the diffraction peak. Plotted in this way, we can begin to identify the outline of a phase transition associated with the formation of the ordered micelles. With the addition of temperature control (implemented but not shown), the AFL could explore the effect of temperature on this phase diagram, with obvious implications on understanding the thermal stability of these formulations. Whereas most real formulations contain more components (e.g., fragrances, colorants, viscosity modifiers, payloads, and secondary surfactants), these data will be used to train ML algorithms that accelerate the mapping of this phase space.[18,19] The algorithms will not only accelerate the phase-mapping process but also, for systems with many components, will prove to enable new studies. Dense grid sampling for such systems scales *exponentially* with the number of components, meaning that for a binary system that could be characterized with 5 measurements, a ternary would require 25, a quaternary 125, and a 10-component system nearly 10 *million* measurements to obtain the same grid spacing. Ten components is a dramatic underestimate of the complexity of many industrial and biological self-assembling systems. The automation approaches presented here promise to provide the ground-truth training data that will enable future advances in understanding.

■ CONCLUSION

AI/ML guided structural screening of formulations is expected to enable significant advances in the ability to engineer particular products while also generating data for a fundamental understanding of the underlying drivers of formulation stability. We present the Autonomous Formulation Laboratory, an open-source platform for autonomous preparation, measurement, and

https://doi.org/10.1021/acs.chemmater.2c03118
Chem. Mater. 2023, 35, 846−852

analysis of liquid mixtures and demonstrate its relevance to several applied systems, including reference nanoparticle data sets, the impact of salt on surfactant morphology, and the construction of simple phase diagrams. The AFL is inherently multimodal, with the support for SAXS, SANS, optical imaging, and UV−vis measurements at present with a road map of several additional complementary techniques. The generation of inherently multimodal reference data with tight control over preparation protocol is expected to prove highly valuable for data fusion techniques and other machine-learning approaches to formulation development.

■ ASSOCIATED CONTENT

Data Availability Statement

Open hardware designs are available on GitHub at https://www.github.com/usnistgov/AFL-hardware. A Python library that abstracts the sample preparation process and the full AFL-automation package are available on GitHub https://www.github.com/usnistgov/AFL-automation.

Supporting Information

The Supporting Information is available free of charge at https://pubs.acs.org/doi/10.1021/acs.chemmater.2c03118.

Notes and instructions for replicating the AFL platform, links to GitHub repositiories of software and open-source hardware components of the AFL, and discussion of clustering details (PDF)

■ AUTHOR INFORMATION

Corresponding Authors

Peter A. Beaucage − *NIST Center for Neutron Research and Materials Science & Engineering Division, National Institute of Standards and Technology, Gaithersburg, Maryland 20899, United States;* orcid.org/0000-0002-2147-0728; Email: peter.beaucage@nist.gov

Tyler B. Martin − *Materials Science & Engineering Division, National Institute of Standards and Technology, Gaithersburg, Maryland 20899, United States;* orcid.org/0000-0001-7253-6507; Email: tyler.martin@nist.gov

Complete contact information is available at: https://pubs.acs.org/10.1021/acs.chemmater.2c03118

Notes

Certain commercial equipment, instruments, materials, suppliers, and/or software are identified in this paper to foster understanding. Such identification does not imply recommendation or endorsement by the National Institute of Standards and Technology, nor does it imply that the materials or equipment identified are necessarily the best available for the purpose.

The authors declare no competing financial interest.

■ ACKNOWLEDGMENTS

The authors thank Aaron Tian and Elizabeth Perez for assistance with software development, Dean DeLongchamp for kind assistance with graphics, and Ron Jones for helpful discussions. Funding for this work was provided by the members of the nSoft industrial consortium (nist.gov/nsoft). P.A.B. thanks the National Research Council for a NIST-NRC postdoctoral fellowship. Use of the Materials Solutions Network at the Cornell High Energy Synchrotron Source (MSN-C) was supported by the U.S. Air Force Office of Scientific Research under Award No. FA8650-19-2-5220. The NIST Center for Neutron Research is supported by the National Institute of Standards and Technology, U.S. Department of Commerce. Official contribution of the National Institute of Standards and Technology; not subject to copyright in the United States.

■ REFERENCES

(1) Lee, B.; Yoon, S.; Lee, J. W.; Kim, Y.; Chang, J.; Yun, J.; Ro, J. C.; Lee, J.-S.; Lee, J. H. Statistical Characterization of the Morphologies of Nanoparticles through Machine Learning Based Electron Microscopy Image Analysis. *ACS Nano* **2020**, *14* (12), 17125−17133.

(2) von Chamier, L.; Laine, R. F.; Jukkala, J.; Spahn, C.; Krentzel, D.; Nehme, E.; Lerche, M.; Hernández-Pérez, S.; Mattila, P. K.; Karinou, E.; Holden, S.; Solak, A. C.; Krull, A.; Buchholz, T.-O.; Jones, M. L.; Royer, L. A.; Leterrier, C.; Shechtman, Y.; Jug, F.; Heilemann, M.; Jacquemet, G.; Henriques, R. Democratising deep learning for microscopy with ZeroCostDL4Mic. *Nat. Commun.* **2021**, *12* (1), 2276.

(3) Zinchuk, V.; Grossenbacher-Zinchuk, O. Machine Learning for Analysis of Microscopy Images: A Practical Guide. *Current Protocols in Cell Biology* **2020**, *86* (1), e101.

(4) Chen, Z.; Andrejevic, N.; Drucker, N. C.; Nguyen, T.; Xian, R. P.; Smidt, T.; Wang, Y.; Ernstorfer, R.; Tennant, D. A.; Chan, M.; Li, M. Machine learning on neutron and x-ray scattering and spectroscopies. *Chemical Physics Reviews* **2021**, *2* (3), 031301.

(5) Doucet, M.; Samarakoon, A. M.; Do, C.; Heller, W. T.; Archibald, R.; Alan Tennant, D.; Proffen, T.; Granroth, G. E. Machine learning for neutron scattering at ORNL*. *Machine Learning: Science and Technology* **2021**, *2* (2), 023001.

(6) Franke, D.; Jeffries, C. M.; Svergun, D. I. Machine Learning Methods for X-Ray Scattering Data Analysis from Biomacromolecular Solutions. *Biophys. J.* **2018**, *114* (11), 2485−2492.

(7) Oviedo, F.; Ren, Z.; Sun, S.; Settens, C.; Liu, Z.; Hartono, N. T. P.; Ramasamy, S.; DeCost, B. L.; Tian, S. I. P.; Romano, G.; Gilad Kusne, A.; Buonassisi, T. Fast and interpretable classification of small X-ray diffraction datasets using data augmentation and deep neural networks. *npj Computational Materials* **2019**, *5* (1), 60.

(8) Wang, B.; Yager, K.; Yu, D.; Hoai, M. In *X-Ray Scattering Image Classification Using Deep Learning*, 2017 IEEE Winter Conference on Applications of Computer Vision (WACV), 24−31 March 2017; IEEE: 2017; pp 697−704.

(9) Bell, R. T.; Beaucage, P. A.; Murphy, M. J.; Connolly, A. B.; Wiesner, U.; Ginley, D.; Van Dover, R. B.; Thompson, M. O. Rapid Identification of Synthetic Routes to Functional Metastable Phases Using X-ray Probed Laser Anneal Mapping (XPLAM) Time−Temperature Quench Maps. *Chem. Mater.* **2021**, *33* (12), 4328−4336.

(10) Suram, S. K.; Xue, Y.; Bai, J.; Le Bras, R.; Rappazzo, B.; Bernstein, R.; Bjorck, J.; Zhou, L.; van Dover, R. B.; Gomes, C. P.; Gregoire, J. M. Automated Phase Mapping with AgileFD and its Application to Light Absorber Discovery in the V−Mn−Nb Oxide System. *ACS Comb. Sci.* **2017**, *19* (1), 37−46.

(11) David, G.; Perez, J. Combined sampler robot and high-performance liquid chromatography: a fully automated system for biological small-angle X-ray scattering experiments at the Synchrotron SOLEIL SWING beamline. *J. Appl. Crystallogr.* **2009**, *42* (5), 892−900.

(12) Lazo, E. O.; Antonelli, S.; Aishima, J.; Bernstein, H. J.; Bhogadi, D.; Fuchs, M. R.; Guichard, N.; McSweeney, S.; Myers, S.; Qian, K.; Schneider, D.; Shea-McCarthy, G.; Skinner, J.; Sweet, R.; Yang, L.; Jakoncic, J. Robotic sample changers for macromolecular X-ray crystallography and biological small-angle X-ray scattering at the National Synchrotron Light Source II. *Journal of Synchrotron Radiation* **2021**, *28* (5), 1649−1661.

(13) Nielsen, S. S.; Moller, M.; Gillilan, R. E. High-throughput biological small-angle X-ray scattering with a robotically loaded capillary cell. *J. Appl. Crystallogr.* **2012**, *45* (2), 213−223.

(14) Murphy, R. P.; Riedel, Z. W.; Nakatani, M. A.; Salipante, P. F.; Weston, J. S.; Hudson, S. D.; Weigandt, K. M. Capillary RheoSANS: measuring the rheology and nanostructure of complex fluids at high shear rates. *Soft Matter* **2020**, *16* (27), 6285−6293.

(15) Wilkinson, M. D.; Dumontier, M.; Aalbersberg, I. J.; Appleton, G.; Axton, M.; Baak, A.; Blomberg, N.; Boiten, J.-W.; da Silva Santos, L. B.; Bourne, P. E.; Bouwman, J.; Brookes, A. J.; Clark, T.; Crosas, M.; Dillo, I.; Dumon, O.; Edmunds, S.; Evelo, C. T.; Finkers, R.; Gonzalez-Beltran, A.; Gray, A. J. G.; Groth, P.; Goble, C.; Grethe, J. S.; Heringa, J.; 't Hoen, P. A. C.; Hooft, R.; Kuhn, T.; Kok, R.; Kok, J.; Lusher, S. J.; Martone, M. E.; Mons, A.; Packer, A. L.; Persson, B.; Rocca-Serra, P.; Roos, M.; van Schaik, R.; Sansone, S.-A.; Schultes, E.; Sengstag, T.; Slater, T.; Strawn, G.; Swertz, M. A.; Thompson, M.; van der Lei, J.; van Mulligen, E.; Velterop, J.; Waagmeester, A.; Wittenburg, P.; Wolstencroft, K.; Zhao, J.; Mons, B. The FAIR Guiding Principles for scientific data management and stewardship. *Scientific Data* **2016**, *3* (1), 160018.

(16) Kim, W.-J.; Yang, S.-M. Effects of Sodium Salicylate on the Microstructure of an Aqueous Micellar Solution and Its Rheological Responses. *J. Colloid Interface Sci.* **2000**, *232* (2), 225−234.

(17) Lam, C. N.; Do, C.; Wang, Y.; Huang, G.-R.; Chen, W.-R. Structural properties of the evolution of CTAB/NaSal micelles investigated by SANS and rheometry. *Phys. Chem. Chem. Phys.* **2019**, *21* (33), 18346−18351.

(18) Noack, M. M.; Yager, K. G.; Fukuto, M.; Doerk, G. S.; Li, R.; Sethian, J. A. A Kriging-Based Approach to Autonomous Experimentation with Applications to X-Ray Scattering. *Sci. Rep.* **2019**, *9* (1), 11809.

(19) Kusne, A. G.; Yu, H.; Wu, C.; Zhang, H.; Hattrick-Simpers, J.; DeCost, B.; Sarker, S.; Oses, C.; Toher, C.; Curtarolo, S.; Davydov, A. V.; Agarwal, R.; Bendersky, L. A.; Li, M.; Mehta, A.; Takeuchi, I. On-the-fly closed-loop materials discovery via Bayesian active learning. *Nat. Commun.* **2020**, *11* (1), 5966.

https://doi.org/10.1021/acs.chemmater.2c03118
Chem. Mater. 2023, 35, 846−852